ELSEVIER

Journal of Alloys and Compounds 452 (2008) 312–324

Journal of ALLOYS AND COMPOUNDS

www.elsevier.com/locate/jallcom

Hydriding and structural characteristics of thermally cycled and cold-worked V–0.5 at.%C alloy

Dhanesh Chandra [a,*], Archana Sharma [a], Raja Chellappa [a], William N. Cathey [a], Franklin E. Lynch [b], Robert C. Bowman Jr. [c], Joseph R. Wermer [d], Stephen N. Paglieri [d]

[a] *University of Nevada, Reno, Reno, NV 89557, USA*
[b] *HCI, 12400 Dumont Way, Littleton, CO 80125, USA*
[c] *NASA Jet Propulsion Laboratory, Mail Stop 79-24, Pasadena, CA 91109, USA*
[d] *Los Alamos National Laboratory, MS-C348, Los Alamos, NM 87545, USA*

Received 31 July 2006; received in revised form 8 November 2006; accepted 8 November 2006
Available online 22 December 2006

Abstract

High pressure hydrides of $V_{0.995}C_{0.005}$ were thermally cycled between β_2- and γ-phases hydrides for potential use in cryocoolers/heat pumps for space applications. The effect of addition of carbon to vanadium, on the plateau enthalpies of the high pressure $\beta_2 + \gamma$ region is minimal. This is in contrast to the calculated plateau enthalpies for low pressure ($\alpha + \beta_1$) mixed phases which showed a noticeable lowering of the values. Thermal cycling between β_2-and γ-phase hydrides increased the absorption pressures but desorption pressure did not change significantly and the free energy loss due to hysteresis also increased. Hydriding of the alloy with prior cold-work increased the pressure hysteresis significantly and lowered the hydrogen capacity. In contrast to the alloy without any prior straining (as-cast), desorption pressure of the alloy with prior cold-work also decreased significantly. Microstrains, $\langle \varepsilon^2 \rangle^{1/2}$, in the β_2-phase lattice of the thermally cycled hydrides decreased after 778 cycles and the domain sizes increased. However, in the γ-phase, both the microstrains and the domain sizes decreased after thermal cycling indicating no particle size effect. The dehydrogenated α-phase after 778 thermal cycles also showed residual microstrains in the lattice, similar to those observed in intermetallic hydrides. The effect of thermal cycling (up to 4000 cycles between β_2- and γ-phases) and cold working on absorption/desorption pressures, hydrogen storage capacity, microstrains, long-range strains, and domain sizes of β_2- and γ-phase hydrides of $V_{0.995}C_{0.005}$ alloys are presented.
Published by Elsevier B.V.

Keywords: Metal hydrides; Domain structure; Thermal cycling; Cold-working; V–0.5 at.%C alloy

1. Introduction

Metal hydrides have been extensively investigated as thermal energy storage media, potentially offering a reversible chemical means of storing and supplying hydrogen for both mobile and stationary systems [1,2]. Hydrides can store more hydrogen per unit volume than liquid or solid hydrogen [3] and have potential applications for heat management systems such as cryocoolers and heat pumps [4–7] besides numerous other applications. By using a suitably matched pair of hydrides with high and low equilibrium pressures, the system can be made to operate continuously to make up the working cycle of a metal hydride heat pump (MHHP). This concept was applied [7] in portable life support systems for space suits in 'Extravehicular Mobility Units' (EMUs), which use such heat pumps. Many applications require constant hydrogen capacity and stability of pressure–temperature properties over a large number of absorption/desorption cycles.

Hydrides of pure vanadium and vanadium alloys are considered to be potential candidates for use in MHHP's [7], hydrogen compressors [8–10], and closed-cycle cryogenic refrigerators [11]. It should be noted that VH_2 has one of the highest volumetric hydrogen density of 160 kg H_2/m^3 although the gravimetric hydrogen density is only ~2 wt%. More recently, Paglieri et al. [12] have investigated vanadium based alloys ($V_{0.95}Ti_{0.05}$ and $V_{0.88}Cu_{0.12}$) coated with palladium for use in hydrogen selective permeable membranes that operate at high temperatures (350–400 °C). For extended use in hydrogen

* Corresponding author. Tel.: +1 775 784 4960; fax: +1 775 784 4316.
E-mail address: dchandra@unr.edu (D. Chandra).

0925-8388/$ – see front matter. Published by Elsevier B.V.
doi:10.1016/j.jallcom.2006.11.078

separation processes, it is necessary that the membranes posses long-term thermal stability and show minimal decrepitation. The alloys and operating conditions are chosen such that β_1, β_2 or γ hydride phases are not formed, i.e., the membranes operates in single phase region allowing maximum hydrogen flux through. For such applications, it is necessary to obtain pressure–composition–temperature (p–c–T) data at very low pressures, without any heat activation cycles to determine the stability regions of the single phase regions. In a recent study, Chandra et al. [13], the low pressure hydriding of $V_{0.995}C_{0.005}$ alloy in the $\alpha-\beta_1$ region was evaluated for development of hydrogen selective membranes at Los Alamos National Laboratory. The low pressure p–c–T data $V_{0.995}C_{0.005}$–H system (338–523 K) suggests that at temperatures beyond 450 K, a stable single α-phase exists that may be suitable for membrane applications.

For pure vanadium, there are two plateaus in the pressure-composition isotherms (PCIs) that correspond to the following reactions:

$\alpha + \beta_1$ plateau ($\sim$ 0.1 Pa at 298 K) :

$$2V(\alpha) + 0.5H_2 \leftrightarrows V_2H(\beta_1) \quad (1)$$

$\beta_2 + \gamma$ plateau ($\sim$ 280, 000 Pa at 298 K) :

$$VH_1(\beta_2) \leftrightarrows VH_2(\gamma) \quad (2)$$

The high-pressure $\beta_2 + \gamma$ plateau is suitable for use in the space related applications being developed by NASA. It is noted that the monohydride (V_2H) and dihydride (VH_2) given in Eqs. (1) and (2) are only nominal compositions (not stoichiometric) and hydrogen content (represented as atomic ratio, $r = H/V$ or atom fraction, $N_H = r/(1+r)$) varies depending upon the solubility at various temperatures. The α-V is BCC and forms monoclinic β_1-V_2H ($0.45 \le r \le 0.7$, $\sim$293 to $\sim$443 K) and as hydrogen content is increased, BCT β_2-VH_1 ($0.45 \le r \le 0.8$, $\sim$293 to $\sim$443 K) and FCC γ-VH_2 ($r \approx 2$, $\sim$298 to $\sim$373 K) are formed. Further details on the crystallographic studies of these phases can be found in Fagerstroem et al. [14].

The thermodynamic properties of V–H system have been the subject of many studies, some of which are briefly mentioned here. In 1959, Kofstad and Wallace [15] reported equilibrium vapor pressure data of V–H system from $N_H = 0.005$–0.33 ($r = 0.005$–0.5) and 438–729 K. In 1969, Veleckis and Edwards [16] reported p–c–T data in the range $N_H = 0.01$–0.33 ($r = 0.01$–0.5), 518.6–827 K, 130 to $\sim 10^5$ Pa, and also reported the relative partial molar enthalpy ($\Delta\bar{H}_H$) and entropy ($\Delta\bar{S}_H$) of hydrogen as a function of N_H. In 1972, Griffiths et al. [17] reported p–c–T data from $N_H = 0.01$ to 0.45 ($r = 0.01$–0.85), 260–460 K, 10^{-5} to $\sim 10^3$ Pa, and also calculated $\Delta\bar{H}_H$ and $\Delta\bar{S}_H$. The last significant p–c–T study in the low pressure region was by Fujita et al. [18] in 1979, who reported data from $N_H = 0.003$ to 0.4 ($r = 0.003$–0.67), 353–773 K, 0.1 to $\sim 10^4$ Pa, and calculated partial molar quantities, as well. In the high pressure, higher hydrogen concentration region, there have been fewer studies. In 1970, Reilly and Wiswall [19] reported PCI data from $N_H = 0.45$ to 0.67 ($r = 0.83$–2), 313–373 K, $\sim 10^4$ to $\sim 10^6$ Pa. Other reported studies include Rummel [20] and Meuffels [21] have also reported p–c–T data in the high and low concentration regimes respectively. Reviews of the V–H systems can be found in Schober [22], and Esayed and Northwood [23], and more references can also be found in the recent thermodynamic assessment of this system [14].

Hysteresis is an important issue in metal hydride applications as it decreases the system wide efficiency. For pure vanadium, it has been found that pressure hysteresis (hydride formation pressure, p_f, is greater than decomposition pressure, p_d) is virtually nonexistent in the low pressure $\alpha + \beta_1$ plateau region [15,16]. In this high pressure $\beta_2 - \gamma$ region, Lynch et al. [24] and Flanagan et al. [25] have showed the presence of pressure hysteresis. In the presence of pressure hysteresis, the ratio (p_f/p_d) is greater than 1 and this ratio typically increases as the hydride undergoes absorption/desorption cycles. The cause of hysteresis has been attributed [26] to irreversible plastic deformation during hydride formation only and therefore assumed that decomposition pressure represented the true equilibrium. However, following the work of Birnbaum et al. [27] to describe solvus hysteresis (terminal hydrogen solubility during absorption, a', is greater than during desorption, a''), Flanagan et al. [28,29] proposed that pressure hysteresis is also due to dislocations creation due to plastic deformation during both hydride formation and decomposition. However, recently this explanation of hysteresis has also been called into question by Schwarz and Khachaturyan [30]. A review of various models of hysteresis can be found in the extensive work of Flanagan et al. [31–33] and Schwarz and Khachaturyan [30]. Regardless of the differences in the proposed theories, hysteresis is generally associated with the plastic deformation and microstrain development in these hydrides due to large changes in the volume.

During use in a MHHP, the vanadium hydride bed is subjected to numerous thermal cycles between β_2- and γ-phases and therefore, the effect of long term thermal cycling on pressure hysteresis and hydriding characteristics is of great interest. Our previous thermal cycling studies on La–Ni based metal hydrides [34–37] have shown intrinsic chemical disproportionation in these hydrides however this is not a concern in VH_x hydrides [38,39]. As we have observed in our earlier studies, thermal cycling (up to 1000 cycles) of VH_x hydrides [38,39] resulted in plastic deformation and sometimes even ruptures of the reactors. For example, a stainless steel reactor containing hydrides of pure vanadium deformed and ruptured after only 200 cycles, although there was little decrepitation of vanadium samples [38]. The absorption hydrogen storage capacity also decreased by 20% and the hysteresis ratio (p_f/p_d) increased from 1.8 to 2.7 after 1000 cycles. It is noted that the increase in hysteresis ratio was primarily due to the increase in absorption pressures while the desorption pressure was relatively unaffected by cycling [38]. Flanagan et al. [25] also studied the effect of cold working on hysteresis in pure vanadium and found that cold working reduced the hydrogen storage capacity of vanadium to $r = 1.65$ from $r = 1.8$ in well annealed sample. In 1995, the thermodynamics of hysteresis in pure vanadium hydrides was reviewed by Kumar and Balasubramaniam [40].

To overcome this problem of microstrain development during γ-phase formation and to determine if the loss in absorption

hydrogen storage capacity can be reduced, it was proposed to add a small amount of carbon (V–0.5 at.% C, $V_{0.995}C_{0.005}$) as an alloying element [41,42]. There have been reports on the stabilization of γ-VH_2 phase to facilitate hydrogen desorption and absorption reactions (reversal of $\gamma \leftrightarrow \beta_2$) by addition of alloying elements [43–45]. Yukawa et al. [46,47] conducted systematic studies on stabilizing both the β- and γ-phases by addition of alloying elements (V–1 mol%M and V–3 mol%M where M is a 3d-, 4d-, or 5d-transition metal) and demonstrated increased stability of γ-phase. Alloying vanadium with carbon may have the potential to minimize the plastic deformation or premature fracture of V-hydride vessels due to large volume changes during $\beta_2 \leftrightarrow \gamma$ transformations [41].

The focus of this study is to evaluate the effect of thermal cycling on the long-term stability of vanadium hydrides operating in the $\beta_2 - \gamma$ region. A detailed analysis of the effects of carbon addition on the thermodynamics (plateau pressures and enthalpies of $\alpha - \beta_1$ and $\beta_2 - \gamma$ plateau regions, and relative partial molar quantities of hydrogen) of low pressure (from data reported by Chandra et al. [13]) and high pressure $V_{0.995}C_{0.005}$ hydrides (this study) were established. The effects of thermal cycling and cold-work on the hydriding pressure, hydrogen capacity, hysteresis, and micro-strain distribution in the crystal lattice of V–0.5 at.%C alloy and associated hydride phases were determined. It was found that the addition of carbon to vanadium prevented the failure of the reactor due to deformation of the container even after hundreds of cycles.

2. Experimental

The experimental work was carried out at University of Nevada, Reno (UNR) and HCI (Littleton, CO). Alloys were arc-melted to form buttons of 1.5 cm diameter. Since powders are difficult to produce from the arc-melted vanadium alloy buttons, finely machined chips of approximately 2 mm in length were obtained by milling and used for hydriding experiments. Vanadium from the U.S. Bureau of Mines, Reno (Lot #11, 99.90% purity) and Teledyne Wah Chang (99.7% purity, plate form) were used for the experimental work. Heat treatment of alloys was performed by wrapping the specimens in tantalum foil, placing the wrapped specimens in a stainless steel envelope sealed in a reduced pressure of argon (below one atmosphere), and heating in a resistance furnace under argon. Pressure–composition isotherm data were obtained with a conventional all metal Sieverts' apparatus. Details of the low pressure experiments are described by Chandra et al. [13] and high pressure experiments are described by Sharma [41]. Hydrogen mass changes were calculated from an empirical equation of state based on National Bureau of Standards Technical Note 617. The vanadium and vanadium alloy samples were placed in a stainless steel reactor on the Sieverts' apparatus where a stainless steel sintered frit filter (nominally 2 μm pore size) protected the vacuum system from fine particle contamination.

The vanadium hydrides were subject to thermal hydriding/dehydriding cycles in an apparatus similar to those described in Lambert et al. [34] except that the reactor was heated using a high intensity quartz lamp and cooled using an air blower. The stainless steel reactor tube was heated to 398 K and cooled to room temperature (298 K) on a 2 h schedule during which a single, complete absorption–desorption cycle (i.e. $\gamma \leftrightarrow \beta_2$ transformation) would take place. Once a desired number of cycles were attained, the sample holder was transferred to the Sieverts' apparatus to make isotherm measurements. The low-pressure $\alpha - \beta_1$ isotherms of V–0.5 at.% C hydrides were obtained from 338 to 523 K. The high pressure $\beta_2 - \gamma$ isotherms were obtained only at three temperatures (298, 323, and 348 K), however, only plateau pressures [41] are available for thermodynamic analysis.

The hydride samples for X-ray diffraction (XRD) experiments were prepared in a special small glove box with a hydrogen atmosphere. The glove box was evacuated to $\sim 10^{-3}$ Torr and back-filled with UHP hydrogen three times prior to opening the VH_x reactor. Powdered samples were loaded into quartz capillaries and sealed by placing the capillaries in a refrigerated aluminum block, maintained at −18 °C inside the hydrogen glove box. The VH_x phases are expected to remain partially charged with hydrogen at this temperature.

A Philips APD 1740 system equipped with a graphite crystal monochromator was used for the X-ray analyses. Copper Kα radiation was used for all experiments. All hydrided samples were sealed into capillaries mixed with a small amount of NBS Si 640b standard combined with quick-setting epoxy. Philips software was used to obtain the *d*-spacings; indexing of the Bragg peaks was performed manually. The lattice parameters were obtained by using a least square refinement method. Although the XRD experiments on hydrides were initially conducted using samples in quartz capillaries, it was found that hydrides exposed to air for several days showed no change in the position or of the relative intensities of the Bragg peaks, suggesting no detectable change in the hydride composition. Before exposing the hydride samples to air, XRD patterns were obtained from samples sealed in capillaries in the hydrogen glove box; the peak positions and relative intensities were the same as those of the samples exposed to air. However, according to the V–H phase diagram [14], VH_2 (γ) phase should decompose to $VH_{0.8}$ (β_2) and V_2H (α) phase at atmospheric pressure and room temperature. One possible explanation is that when the samples are exposed to air at low temperature a thin oxide layer may form, retarding or stopping the decomposition [48–50]. Reilly and Wiswall [19] have reported very slow decomposition of such hydrides in air, but we did not observe any change in the X-ray powder diffraction patterns even after 2 months, which gave us adequate time to conduct the XRD experiments. Many X-ray diffraction patterns of vanadium hydrides were obtained, shortly after being exposed to air. The main reason to remove the sample from the capillary was to reduce the data collection time and to increase the signal to noise ratio due to scattering from the quartz capillary.

The micro-strain analyses were performed using the Philips line profile program [51]. Measurements of strain and domain size (*D*) in the lattice were performed by first selecting appropriate sets of two peaks collected over a 2θ range, such as (1 1 0), (2 2 0). The reference peaks for Stokes corrections from the standard were obtained by appropriate pattern treatment, i.e., background subtraction and correction of peak position errors via internal NBS Si standard. Then, cosine coefficients for both reflections were obtained in order to perform line profile analyses. By applying the Stokes correction, the true broadening of the peak and the sine and cosine coefficients of the true broadened function were obtained. The root-mean-squares microstrain, $\langle \varepsilon^2 \rangle^{1/2}$, and domain sizes were calculated using Fourier analysis methods such as the Warren–Averbach method [34,52]. The peak positions of the Bragg reflections of these hydrides did not match the annealed vanadium standard but platinum and indium peaks matched the peak positions of selected $VH_{0.8}$ (β_2) and VH_2 (γ) phases, respectively; that were used in this study for instrumental broadening. The peak profile analyses of the γ-phase were performed by using Voigt functions [53] because pairs of the peaks were not available due to overlap with β_2-phase peaks.

The dehydrogenation experiments were performed in a Perkin-Elmer four differential thermal analyzer (DTA) because simple evacuation did not successfully remove the hydrogen from the cycled vanadium hydrides to form α-phase.

3. Results and discussion

3.1. Effect of carbon addition on hydride thermodynamics

3.1.1. Plateau pressures ($\alpha + \beta_1$ and $\beta_2 + \gamma$ regions)

Pressure–composition absorption isotherms of V–0.5 at.%C alloy ($V_{0.995}C_{0.005}$) taken at several temperatures (338, 398, 423, 448, 473, and 523 K) from Chandra et al. [13] are superimposed with a compilation of *p–c* isotherms from the previous studies on pure V in Fig. 1. A preliminary analysis of the *p–c–T* data of $V_{0.995}C_{0.005}$ in Fig. 1 shows that β_1 hydride phase may not form beyond ~450 K. Tentative phase boundaries determined for $V_{0.995}C_{0.005}H_x$, from the low pressure data have

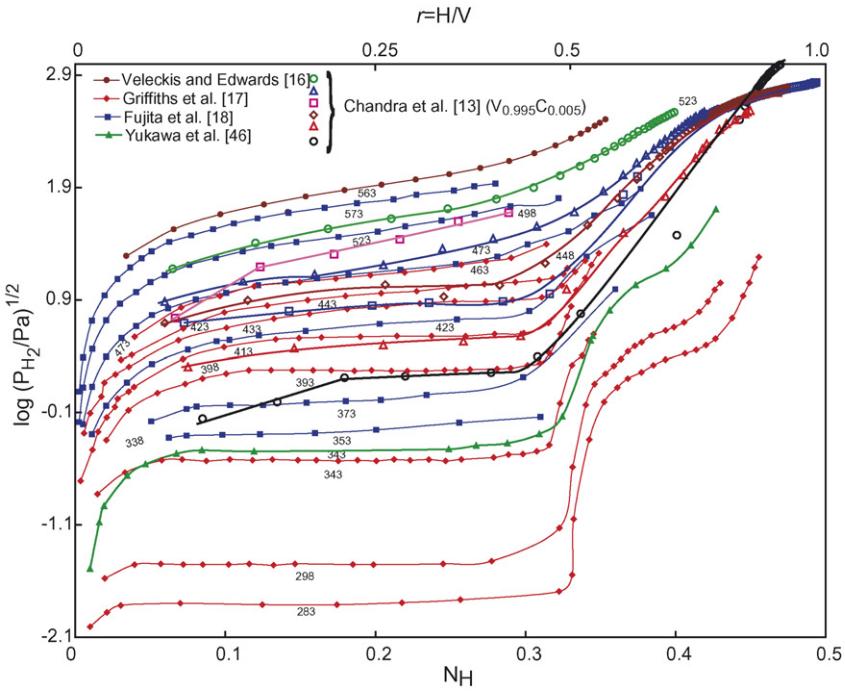

Fig. 1. Pressure–composition isotherms of V–0.5 at.%C taken at several temperatures showing variation of $\alpha - \beta_1$ plateau pressures from Chandra et al. [13] (darker lines) and comparison with Veleckis and Edwards [16], Griffiths et al. [17], Fujita et al. [18], Yukawa et al. [46] data of pure V. The plateau pressures of V–0.5 at.%C are slightly higher than that of pure V.

been discussed by Chandra et al. [13]. It is noted that more data is desired to conclusively establish the changes in solidus lines due to alloying. It is pointed out that only selected temperatures (<573 K) are shown in order to avoid overloading the figure with symbols. The data from Kofstad and Wallace [15] are not shown here for the sake of clarity as the isotherms crossed with other data. It can be seen that the absorption pressures for $V_{0.995}C_{0.005}$ alloy are higher than that for pure V. However, the pressures for 338 K for $V_{0.995}C_{0.005}$ alloy from Chandra et al. [13] seem unusually higher and the reason for this is not clear. At higher temperatures (for e.g. 563 K), the pressures reported by Veleckis and Edwards [16], are higher than that reported by Fujita et al. [18]. Otherwise, there is a good correspondence among the pure vanadium data of Griffiths et al. [17], Fujita et al. [18], and the data for $V_{0.995}C_{0.005}$ alloy. Although, Chandra et al. [13] did obtain any desorption data for $V_{0.995}C_{0.005}H_x$, it has been shown previously that there is virtually no hysteresis in the low pressure $\alpha - \beta_1$ region for pure vanadium [15,16].

In Fig. 2, the high pressure isotherm of are $V_{0.995}C_{0.005}$ alloy at 298 K from this study, is superimposed with the high pressure isotherms of vanadium hydrides from Reilly and Wiswall [19] and Yukawa et al. [46]. Desorption isotherms were measured at 298, 323, and 348 K on a sample of $V_{0.995}C_{0.005}$ alloy that was annealed at 1200 °C for 24 h but only the mid-plateau pressures 258 kPa (298 K), 912 kPa (323 K) and 2710 kPa (348 K) are available [41]. The plateau pressure (at 343 K) reported by Yukawa et al. [46] for $\beta_2 + \gamma$ mixed phase region is slightly higher than that of Reilly and Wiswall [19]. The high pressure data of Luo et al. [54] does agree in terms of the plateau pressure, but the maximum H/M ~1.62 is lower than that of Reilly and Wiswall [19] (H/M = ~2). The solubility limit in the higher concentration for $V_{0.995}C_{0.005}$ alloy is H/M ~1.95 at 298 K. The reason for this discrepancy was explained as partial activation of the sample [54]. However, the calorimetric data from Luo et al. [54] is considered accurate for plateau enthalpies. We also had similar experiences when hydriding highly strained V–0.5 at.%C alloy; i.e., the maximum H/M is low [41]. It has also been previously shown by Reilly and Wiswall [19] that the plateau pressures are affected significantly by the purity of vanadium.

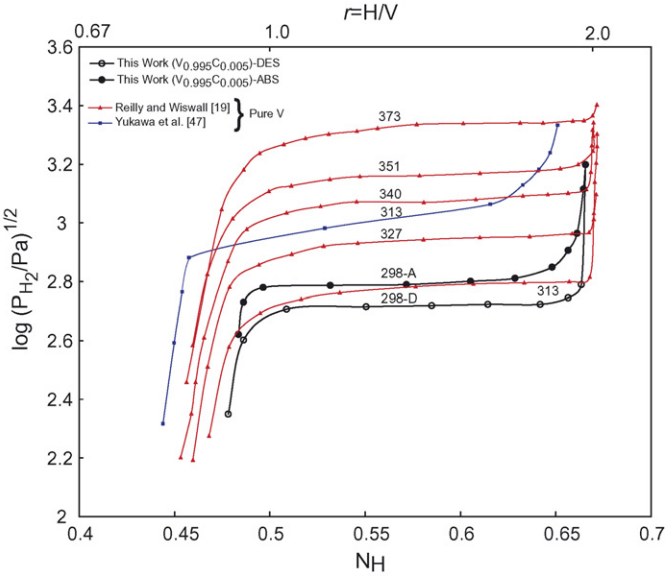

Fig. 2. High pressure isotherm of V–0.5 at.%C at 298 K along with the high pressure isotherms of pure V from literature to show the $\beta_2 - \gamma$ plateau region.

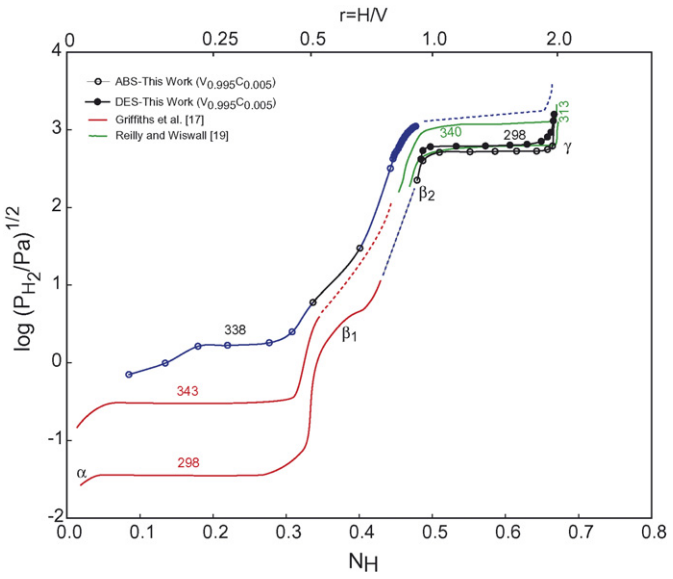

Fig. 3. Low- and high-pressure isotherms of pure vanadium from this work, along with high pressure isotherm of V–0.5 at.%C at 298 K to show the α-, $\alpha+\beta_1$-, $\beta_1+\beta_2$-, and $\beta_2+\gamma$-phase regions.

In Fig. 3, a combination of the isotherms of low pressure and high pressure hydride of $V_{0.995}C_{0.005}$ alloy are shown. Although, a similar plot was in shown in Chandra et al. [13], we find it illustrative to redraw such a composite plot to show the two plateau regions for $V_{0.995}C_{0.005}$–H system. The plateau pressures for the $\alpha-\beta_1$- and $\beta_2-\gamma$-phases 0.1 Pa and 280,000 Pa at 298 K showing a $\Delta P \sim 10^7$ Pa. The isotherms for the high-pressure hydride were obtained at 298 K after 10 activation cycles [41], whereas the isotherms for the low-pressure hydride were taken at 338 K are from Chandra et al. [13], without any temperature activation. The $\alpha-\beta_1$ plateau region occurs only up to H/M (r) $\cong 0.5$ until the formation of V_2H β_1-phase is complete, after which there is a $\beta_1-\beta_2$ solid solution region [14]. Low-pressure data were not obtained at 298 K for this alloy; therefore, the pure vanadium low-pressure data ($\alpha-\beta_1$ region) at 298 and 343 K from Griffiths et al. [17] along the high pressure data ($\beta_2-\gamma$ region) from Reilly and Wiswall [19] (313 and 340 K) to show the progressing trend of hydrogenation of pure vanadium from low to high pressures. Data was not collected between 100 and 31,600 Pa, so a dotted line is drawn to suggest the continuity of the isotherm to the higher pressure region data. The plateau region $\beta_2-\gamma$ exists from $r = \sim 0.8$ to 2.0, and the dissociation plateau pressures in the $\beta_2-\gamma$ plateau region are 200 and 280 kPa for pure vanadium and $V_{0.995}C_{0.005}$ alloy, respectively. This 40% increase in the plateau pressure for $V_{0.995}C_{0.005}$ alloy is reasonable compared with the results of Cantrell and Bowman [42] and also reported by Yukawa et al. [46,47] for V-based alloys.

3.1.2. Thermodynamic properties

The low pressure data from Griffiths et al. [17] and Fujita et al. [18], the high pressure data from Reilly and Wiswall [19], and the enthalpy data from Luo et al. [54] are considered reliable and most comparisons of the calculated thermodynamic properties from the present study will be made with these earlier studies. The equilibrium van't Hoff plot and the plateau enthalpy and entropy for the $\alpha-\beta_1$ region were presented by Chandra et al. [13]. In this section, a detailed thermodynamic analysis of both $\alpha-\beta_1$ and $\beta_2-\gamma$ regions The van't Hoff plots obtained from the plateau pressures for $\alpha-\beta_1$ and $\beta_2-\gamma$ mixed phase regions are shown in Fig. 4. These equilibrium equations along with the calculated ΔH_{plat} and ΔS_{plat} are listed in Table 1 and compared with the values for pure vanadium reported in literature. As mentioned earlier, the plateau pressures for the isotherm at 338 K are unusually higher and it can be seen that including the plateau pressure from this temperature would result in smaller slope, ΔH_{plat}, and ΔS_{plat} (magnitude will be affected more as it depends on the plateau pressure). At this time, the reason for this higher pressure is not clear and further experiments are desired in this temperature range (323–373 K). Therefore, only plateau pressures from 398, 423, to 448 K were used for determining ΔH_{plat}, and ΔS_{plat}. The change in entropy for both high and low pressure plateaus are referred to 101,325 Pa (1 atm). It is pointed out that for calculation of the ΔH_{plat}, and ΔS_{plat} for $\alpha-\beta_1$ region, we used the interpolated pressure values at $N_H = 0.2$ ($r = 0.25$), and for $\beta_2-\gamma$ region, we used the pressures at $N_H = 0.6$ ($r = 1.5$). The interpolated values at $N_H = 0.2$ ($r = 0.25$) for 473, 498, and 523 K are also shown in the van't Hoff plot. Although, at these temperatures, $V_{0.995}C_{0.005}H_x$ may

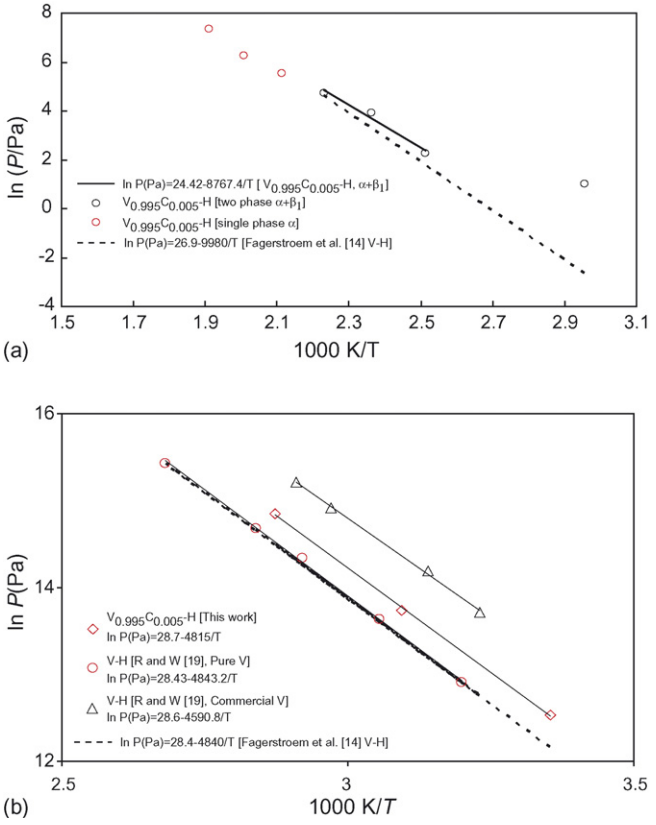

Fig. 4. (a) Van't Hoff plots of the $\alpha+\beta_1$ plateau region for V–0.5 at.%C–H [13] compared with the plot for V–H. The decrease in slope and the intercept resulted in a decrease in the enthalpy and entropy. The pressure measurement at 338 K was not used to determine the fitted equation. (b) Van't Hoff plots of the $\beta_2+\gamma$ plateau region for V–0.5 at.%C–H (this work) compared with the plots for V–H from other references.

Table 1
Compilation of van't Hoff equations for ($\alpha+\beta_1$) and ($\beta_2+\gamma$) plateau regions of hydrogen in pure vanadium and V–0.5 at.%C

System	Plateau	van't Hoff equation	$-\Delta H_{plat}$ (kJ (mol H_2)$^{-1}$)	$-\Delta S_{plat}$ (J K^{-1} (mol H_2)$^{-1}$)	T_{range} (K)
$V_{0.995}C_{0.005}H_x$[a]	**$\alpha+\beta_1$**	**$\ln P$ (Pa) = 24.42 − 8767.4/T**	**72.9**	**107.2**	**398–448**
V–H[b]	$\alpha+\beta_1$[b]	$\ln P$ (Pa) = 26.9 − 9980/T	83	127.8	283–313
V–H[c]	$\alpha+\beta_1$	–	77.2	114.6	353–373
V–H[d]	$\alpha+\beta_1$	–	81.2 ± 0.5	122.6	323 K
	$\beta_2+\gamma$		38.2 ± 0.3	140	
$V_{0.995}C_{0.005}H_x$[a]	**$\beta_2+\gamma$**	**$\ln P$ (Pa) = 28.7 − 4815/T**	**40**	**142.4**	**298–348**
V–H[a]	$\beta_2+\gamma$	$\ln P$ (Pa) = 28.43 − 4843.2/T[1e]	40.3	140.6	312–373
		$\ln P$ (Pa) = 28.6 − 4590.8/T[2e]	38.2	142	310–344

[a] This work (in bold).
[b] The van't Hoff equation is from Fagerstroem et al. [14] who used data from Griffiths et al. [17].
[c] Fujita et al. [18].
[d] The reaction calorimetry data from Luo et al. [54]. $-\Delta S_{plat}$ was calculated using plateau pressure from Griffiths et al. [17].
[e] Reilly and Wiswall [19] have reported three van't Hoff plots for pure (1), commercial (2).

be single α-phase, it is interesting to see these pressures fall on the van't Hoff slope. It can also be seen from Table 1 that in the higher pressure $\beta_2+\gamma$ region, addition of 0.5 at.% carbon to vanadium produced only a 0.24 kJ (mol H_2)$^{-1}$ change in ΔH_{plat}, whereas commercial vanadium with a larger impurity content reduced ΔH_{plat} by 2.2 kJ (mol H_2)$^{-1}$. The alloying effect of carbon is more pronounced at low pressure $\alpha+\beta_1$ regions, as ΔH_{plat} is reduced from 81.2 (83 [17]) kJ/mol H_2 to 72.9 kJ/mol H_2. Correspondingly, the relative changes in ΔS_{plat} are also higher in the $\alpha+\beta_1$ region due to addition of carbon than in $\beta_2+\gamma$ region.

The relative partial molar Gibbs energy (chemical potential), enthalpy, and entropy of hydrogen relative to gaseous diatomic hydrogen at 101,325 Pa (1 atm), at a given atom fraction (condensed phase) are defined as follows:

$$\Delta\bar{G}_H = \bar{G}_H - \frac{1}{2}G^{\circ}_{H_2} = \frac{1}{2}R\ \ln\ P_{H_2} \tag{3}$$

$$\Delta\bar{H}_H = \bar{H}_H - \frac{1}{2}H^{\circ}_{H_2} = \frac{1}{2}R\left(\frac{\partial(\ln\ P_{H_2})}{\partial(1/T)}\right)_{N_H} \tag{4}$$

$$\Delta\bar{S}_H = \frac{\Delta\bar{H}_H - \Delta\bar{G}_H}{T} \tag{5}$$

Further details of derivation of Eqs. (3)–(5) can also be found in Fujita et al. [18]. Here, the partial molar enthalpy of hydrogen ($\bar{H}_H$) is related to the chemical potential ($\mu_H = \bar{G}_H$) by the Gibbs–Helmholtz equation:

$$\bar{H}_H = \left(\frac{\partial(\bar{G}_H/T)}{\partial(1/T)}\right)_{N_H, P_{H_2}} \tag{6}$$

Using Eqs. (3)–(5), we obtain the following simple relation between P_{H_2}, $\Delta\bar{H}_H$, and $\Delta\bar{S}_H$:

$$\ln\ P_{H_2} = \frac{2\Delta\bar{H}_H}{RT} - \frac{2\Delta\bar{S}_H}{R} \tag{7}$$

Therefore, by plotting $\ln\ P_{H_2}$ versus $1/T$ for a fixed composition N_H, we can obtain relative partial molar enthalpy and entropy of hydrogen in the solid phase. These quantities are important interpret phase stabilities of the various phases as well as to identify second order transitions [17,54]. The increasing values of $\Delta\bar{H}_H$ can also be simply correlated to increasing vapor pressure of hydrogen [15]. The integral quantities such as ΔH_f can also be determined by using the Gibbs–Duhem equation [15,16] however we do not go into the details of such a calculation due to lack of data in the infinite dilution region. The $\Delta\bar{H}_H$ and $\Delta\bar{S}_H$ for V–0.5 at.%C alloy is shown in comparison with the literature data for pure vanadium in Fig. 5a and b. The phase boundary limiting lines are taken from Luo et al. [54]. It can be seen that the reaction calorimetry data shows a nice horizontal trend in the mixed phase region however the enthalpy values from the *p–c–T* type data show a sloping increase in the enthalpy values. The values for $\Delta\bar{H}_H$ and $\Delta\bar{S}_H$ for V–0.5 at.%C alloy are slightly lower than the values for pure vanadium. As expected, beyond the solidus of $\alpha+\beta_1/\beta_1$, there is significant drop in the $\Delta\bar{H}_H$ values and this trend can be seen for both pure vanadium (Luo et al. [54]) and $V_{0.995}C_{0.005}$ alloy. In the high pressure region, we have calculated $\Delta\bar{H}_H$ and $\Delta\bar{S}_H$ values using the data from Reilly and Wiswall [19]. The only data for $V_{0.995}C_{0.005}H_x$ from this study are the plateau values from $\beta_2+\gamma$ region. For pure vanadium, extrapolation of $\Delta\bar{H}_H$ and $\Delta\bar{S}_H$ to infinite dilution [17] gives $\Delta\bar{H}^{\circ}_H = -(33.8 \pm 0.4)$ kJ (mol H)$^{-1}$ and $\Delta\bar{S}^{\circ}_H = -(26.5 \pm 0.3)$ kJ (mol H)$^{-1}$. Similar values have been reported by Luo et al. [54], and others. Furthermore, a straight line extrapolation assuming the validity of Sievert's law is considered valid from $N_H = 0.01$ or lower and since, we did not obtain pressure values below $N_H = 0.08$ (0.06 for some temperatures) to perform such an extrapolation.

In summary, the effect of addition of small amount of carbon has relatively more effect in the low pressure $\alpha+\beta_1$ region than in the high pressure $\beta_2+\gamma$ region. There are higher absorption pressures and further lowering of ΔH_{plat} and ΔS_{plat} in the $\alpha+\beta_1$ region than in the high pressure $\beta_2+\gamma$ region. It is well known that a lower ΔH_{plat} implies lower thermochemical stability, higher dissociation pressure, and lower decomposition temperature. Therefore, addition of small amount of carbon is somewhat beneficial to the low pressure hydriding thermodynamics. Due to the relatively unchanged values of ΔH_{plat} in the high pressure $\beta_2+\gamma$ region, there is relatively little effect of addition of carbon on the thermodynamics. However, the carbon

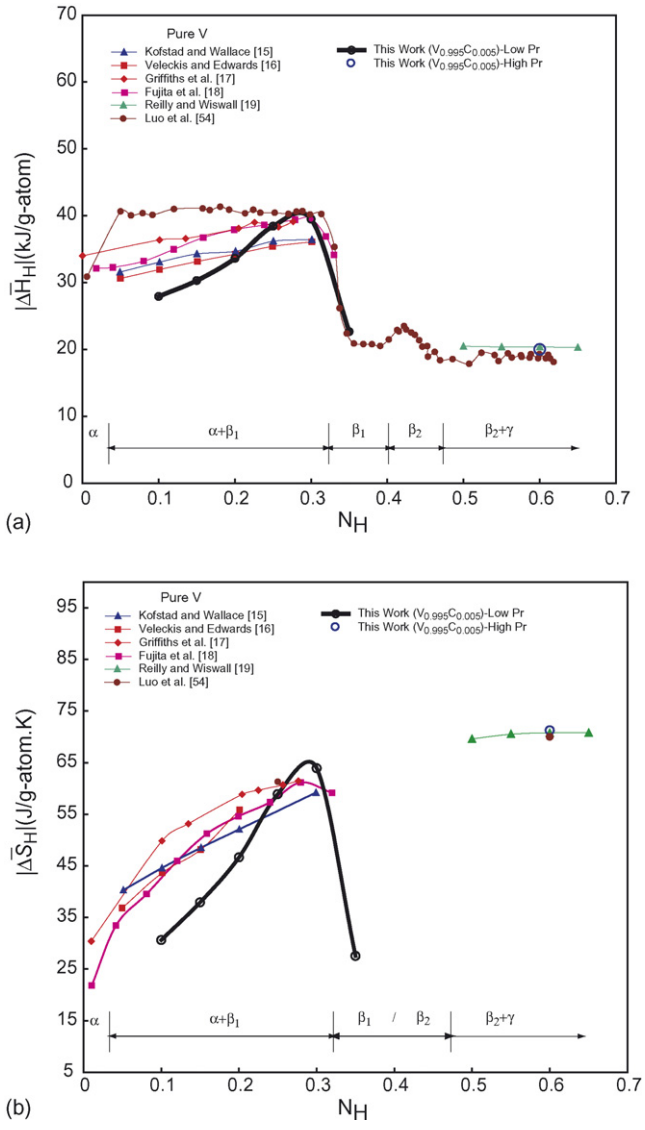

Fig. 5. (a) Relative partial molar enthalpy and (b) relative partial molar entropy of hydrogen as a function of atom fraction of hydrogen in the condensed phase.

is used for pinning the dislocation as this alloy is susceptible to plastic deformation, and this small amount of carbon may be very effective in pinning dislocations. As discussed by Chandra et al. [13], the XRD characterization of the *low pressure* V–0.5 at.%C sample before and after the hydriding up to 10,000 Torr showed very little change in either the peak width or the Bragg angle, indicating that there is nearly complete reversal of the β_1- or β_2-phases to a V–0.5 at.%C alloy. The SEM micrographs [13] of the V–0.5 at.%C alloy after experiments for 8 months showed that there is no decrepitation of the alloy except for some fissure formation.

3.2. Effect of thermal cycling

3.2.1. Plateau pressures and microstrains

It is of great interest to know the effect of long term thermal cycling of the metal hydrides (while in use as membranes and in MHHP) on the hydrogen absorption and desorption pressures as well as the hydrogen storage capacities. In this study, we have determined the effect of thermal cycling on the high pressure hydriding behavior of V–0.5 at.%C alloy. We focus on the high pressure mixed phase region ($\beta_2 - \gamma$) as the high pressure hydride has the greater potential for applications such as cryocoolers, membranes, etc. Furthermore, the pressure hysteresis effect is minimal in low pressure $\alpha - \beta_1$ region of pure vanadium. The V–0.5 at.%C hydride was subjected to prolonged thermal cycling between β_2 and γ in the range of 298–397 K up to 4000 cycles. Isotherms obtained at 298 K after 1, 778, 1345, 1633, and 4000 thermal cycles are shown in Fig. 6. Absorption plateau pressures increased noticeably as a function of cycles however, desorption pressures did not change significantly, even after 1633 cycles. The hysteresis and slope of the absorption plateaus are very pronounced for all of the thermally cycled samples. Further discussion on the effect of thermal cycling on the pressure hysteresis is given later.

To perform phase composition analyses on the V–0.5 at.%C hydrides, the cycled hydrides in the sealed sample holders were taken to the glove box under high hydrogen pressure (upper limit of the γ-phase). The pressure was released slowly inside the hydrogen glove box and the powder samples were loaded in capillaries and sealed at ambient pressure. It is expected that the cycled samples at higher pressures may revert along the isotherm back to the β_2-phase. XRD patterns in Fig. 7 of the hydrides cycled 1 and 778 times reveal that both β_2- and γ-phase Bragg peaks were observed in the patterns. Qualitative analyses showed that the amount of γ-phase, $\gamma/(\beta_2 + \gamma)$, decreased from 0.9 to 0.1, based on changes in Bragg peak intensities and internal standards. Reilly and Wiswall [19] have previously suggested that impurities influence the decomposition rate of the γ-phase because these impurities can cause disorder in the hydrogen sub-lattice of the vanadium dihydride phase. Enhanced hydrogen diffusion could account for the reduced concentration of the γ-phase in the thermally cycled samples. X-ray diffraction patterns of $VH_{0.8}$ (β_2) BCT phase in the mixture of $\beta_2 + \gamma$,

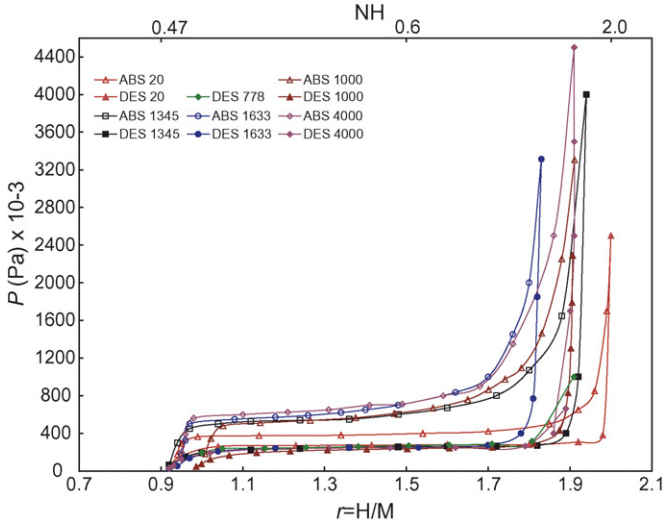

Fig. 6. Isotherms showing the effect of thermal cycling on the plateau absorption and desorption pressures measured at 298 K. Absorption data for 778 cycles is not available.

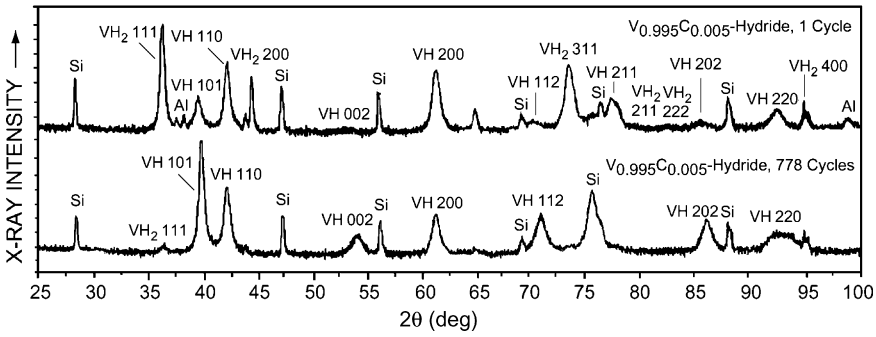

Fig. 7. X-ray diffraction patterns of V–0.5 at.%C hydrides cycled 1 and 778 times.

after 1 and 778 cycles, showed broadened Bragg peaks as compared to the instrumental broadening. However, the relative peak broadening decreased after thermal cycling because of an effect resembling annealing. Line profile analyses performed using the Warren–Averbach model on these materials showed that the microstrains of the $VH_{0.8}$ phase decreased slightly from $3.5\ (\pm 0.10) \times 10^{-3}$ at 1 cycle to $2.2\ (\pm 0.14) \times 10^{-3}$ after 778 cycles; a 35% decrease. There was a corresponding increase in domain sizes from 10.5 to 21 nm in the principal [1 0 1] direction. The analyses for the β_2-phase of thermally cycled samples are presented in Fig. 8(a) and (b). The line broadening analyses of the VH_2 (γ) (cubic fluorite) phase in the mixture of $\beta_2 + \gamma$ product also showed a microstrain, $\langle \varepsilon^2 \rangle^{1/2}$, decrease from 3.317×10^{-3} to 1.422×10^{-3}; a 57% decrease in the principal [1 1 1] direction.

The microstrains described above are in addition to the long-range tensile or compressive strains present in the lattice of the hydrides after thermal cycling. The lattice parameters for V–0.5 at.%C alloy and pure vanadium are given in Table 2. The net change in the lattice parameters in Table 2 after thermal cycling between γ- and β_2-phases reflect the long-range residual strains (ε) in the hydride phases. Highly anisotropic long-range strains are observed in the β_2-phase after cycling. Long-range compressive strains are developed in the c-direction; $\varepsilon_{\beta_2[0\ 0\ 1]}$ or $(\Delta c/c)\beta_2 = -14 \times 10^{-3}$ but tensile strains $\varepsilon_{\beta_2[1\ 0\ 0]}$ or $(\Delta a/a)\beta_2 = +0.19 \times 10^{-3}$ are developed in the a-direction. The related $\varepsilon_{\beta_2[1\ 0\ 1]}$ or $(\Delta d/d)\beta_2 = -6.1 \times 10^{-3}$. Compressive strains are also developed in the cubic γ-phase after cycling. In the cubic γ-phase, residual compressive strain, $\varepsilon_{\gamma[101]} = -2.13 \times 10^{-3}$, and a tensile strain, $\varepsilon_{\gamma[111]} = +0.19 \times 10^{-3}$, were observed. The structural properties of α-phase obtained from the V–0.5 at.%C hydride after 1 and 778 cycles (exposed to air containing γ and β_2 binary phases) show that $\gamma \rightarrow \beta_2 \rightarrow \alpha$-phase decomposition requires heating of the sample and cannot be attained by simple evacuation methods as used on $LaNi_5$ and other intermetallics [55,56].

3.2.2. *Differential thermal analyses*

Dehydrogenation should be attained without recrystallization at temperatures below 673 K, judging by the high melting point of vanadium (2173 K). It is likely that some recovery (annealing) processes might take place during the dehydrogenation. Complete dehydrogenation of the β_2- and γ-phases was attained by heating the sample in a differential thermal analyzer (DTA). Heating the once cycled $\beta_2 - \gamma$ binary phases in DTA showed one endotherm of the $\gamma \rightarrow \beta_2$ transition with an onset temperature of ~473 K and is given in Fig. 9(a), trace A. The other endotherm at ~593 K was that of the β_2 and $\beta_1 \rightarrow \alpha$ transition. The V–H phase diagram shows that the $\gamma \rightarrow \beta_2$ transition occurs at 375 K and $\beta_2 \rightarrow \alpha$ at 470 K [14]; the increases in phase transition temperature were attributed to the addition of carbon to vanadium. Indeed, other investigators have

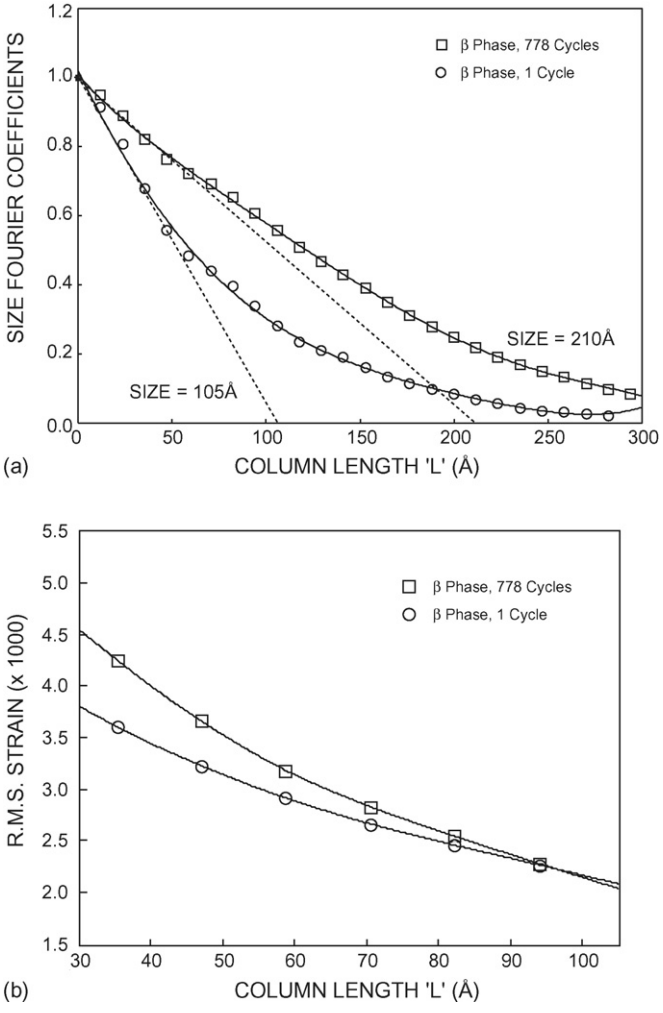

Fig. 8. (a) Effective domain size, D, and (b) microstrain, along [1 0 1] of the β-phase hydrides of V–0.5 at.%C after 1 and 778 cycles.

Table 2
Lattice parameters of vanadium and V–0.5 at.%C α-phases and their β̃ and γ-phase hydrides in thermally cycled and cold-worked conditions

Hydrides	α-Phase (bcc) a(Å)	Thermally cycled and cold-worked	β-Phase (BCT)				γ-Phase (FCC)	
			a (Å)	c (Å)	c/a	V (Å^3)	a (Å)	V (Å^3)
Pure vanadium[a]	3.0279 ± 0.0013							
V–0.5 at.%C[a]	3.0229 ± 0.0013	V–0.5 at.%C (1 cycle)	3.0241 ± 0.0019	3.4360 ± 0.0020	1.1362	31.42	4.2685 ± 0.0005	77.77
V–0.5 at.%C[b]	3.0270 ± 0.0016	V–0.5 at.%C (778 cycles)	3.0247 ± 0.0009	3.3876 ± 0.0014	1.1199	30.99	4.2594 ± 0.0001	77.28
V–0.5 at.%C[c]	3.0311 ± 0.0025	V–0.5 at.%C (cold-worked)	3.0337 ± 0.0050	3.4062 ± 0.0056	1.1222	31.35	4.2760 ± 0.0018	78.18

[a] Before hydriding.
[b] Dehydrogenated after one hydriding cycle.
[c] Dehydrogenated after 778 hydriding cycles.

observed variations in decomposition temperature (e.g. from ∼273 to 473 K) [10]. Essentially, complete dehydrogenation of the 778-cycled hydride has also been attained; the DTA trace B in Fig. 9(b) shows an endotherm of the $\gamma \rightarrow \beta_2 \rightarrow \alpha$ transition with an onset temperature of 593 K, but the endotherm for the $\gamma \rightarrow \beta_2$ decomposition is not observed in this DTA trace. This may be attributed to the rather very small concentration of the residual γ-phase in the hydride samples cycled 778 times, based on the XRD pattern in Fig. 7. By reheating the sample in the DTA, complete dehydrogenation was confirmed since no endotherms were observed as shown in Fig. 9(c).

X-ray diffraction analyses of the dehydrogenated alloy obtained after heating the samples in the DTA confirmed formation of terminal α-phase from the 1 and 778 cycled $\beta_2 - \gamma$-phase hydrides. However, the Bragg peaks of the terminal α-phase were broadened due to residual microstrains and domain size effects despite heating to 400 °C. As given in Fig. 10(a), the domain size of the dehydrogenated α-phase decreased from 195 Å in the sample thermally cycled once to 115 Å in the sample cycled 778 times, amounting to a 40% decrease in the domain size along the [1 1 0] direction. The corresponding residual microstrains given in Fig. 10(b) in the α-phase increased from 2.05 $(\pm 0.10) \times 10^{-3}$ in the sample cycled once to 2.2 $(\pm 0.10) \times 10^{-3}$ after 778 cycles, both measured at $L = 100$ Å in the [1 1 0] direction. This small increase in the microstrain in the cycled hydride is associated with decreased hydrogen capacity similar to that observed for intermetallic hydrides such as $LaNi_5$ [55,56]. A comparative listing of the microstrains developed in the α-, β- and γ-phases, before and after, thermal cycling and cold working are given in Table 3. In the dehydrided α-phases, the increases in microstrains after 1 cycle were not significantly greater than for hydride cycled 778 times. These results clearly show that the significant amount of microstrain developed in the lattice during the initial activation cycles may actually be relaxed by subsequent cycling. Also, these results are similar to those observed in the thermally cycled AB_5 hydrides by Lambert et al. [34], Uchida et al. [57], Nomura et al. [58], and Josephy et al. [59]. For example, Lambert et al. [34] showed that the majority of the microstrains in the α-phase of $La_{0.9}Gd_{0.1}Ni_5$ were developed during the initial activation. Small increases in microstrain may be attributed to the intrinsic nature of plastic behavior in metals and alloys. However, it should be noted that the thermal cycling in vanadium alloys was performed between the β and γ hydrides rather than cycling between the β and α hydride phases as in the case of $LaNi_5$ and its substituted alloys.

3.2.3. Hysteresis in thermally cycled hydrides

Thermal cycling effects on pressure hysteresis are summarized in Fig. 11(a) which shows changes in the hysteresis ratio (p_f/p_d) and the effective hydrogen storage capacity (H/M) of the hydride phases as a function of the number of cycles. The curves are hand drawn to illustrate the trends in the changes in hysteresis ratio and H/M. The hysteresis ratio increased from 1.4 to 2.9 (4000 cycles). The value after 1000 cycles is ∼2.7. It is interesting to note that for VH_x [38] also the ratio was also 2.7 (increasing from 1.8) after 1000 cycles. The effective hydrogen

Table 3
Summary of domain size and microstrain in α-, β-, and γ-phases of the V–0.5 at.%C alloy in thermally cycled and cold worked condition

Material	Phase	Direction	Domain size (D) (Å)	Microstrain $\langle \varepsilon^2 \rangle^{1/2} \times 10^3$
	α[a] (1 cycle)	[1 1 0]	195[a]	2.05
	α[a] (778 cycles)		115	2.2
Thermal cycling	β (1 cycle)	[1 0 1]	105	3.5
	β (778 cycles)		210	2.2
	γ (1 cycle)	[1 1 1]	452	3.3
	γ (778 cycles)		292.7	1.4
Cold working	α[b]	[1 1 0]	210	2.0
	β	[1 0 1]	200	2.2
	γ	[1 1 1]	438	2.4

[a] After dehydrogenation.
[b] Alloy before dehydriding.

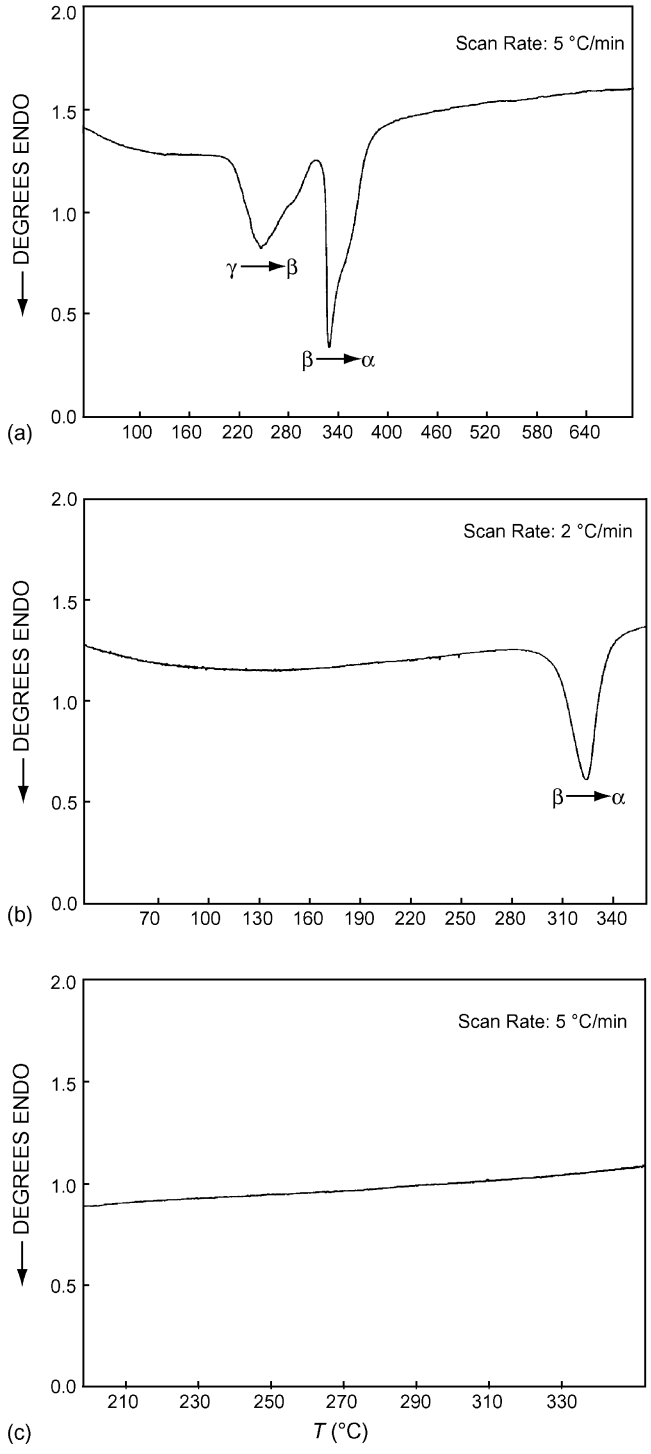

Fig. 9. DTA traces before hydrogenation showing the phase transitions occurring during heating. (a) V–0.5 at.%C hydride cycled once showing $\gamma \rightarrow \beta$ transition with an onset temperature of 473 K and $\beta \rightarrow \alpha$ transition with an onset temperature of 583 K. (b) Hydride cycled 778 times showing $\beta \rightarrow \alpha$ transition with an onset temperature of 583 K. (c) Hydride cycled 778 times after dehydrogenation, confirming complete transformation to the α-phase.

storage capacity decreased from 2 to 1.83 (1633 cycles) before increasing to 1.96 (4000 cycles); perhaps this may under experimental uncertainty. It is noted that the effective hydrogen storage capacity loss after 1000 cycles in VH_x is about 20% (from 2 to 1.6) while in $V_{0.995}C_{0.005}H_x$ it reduced by only 5%

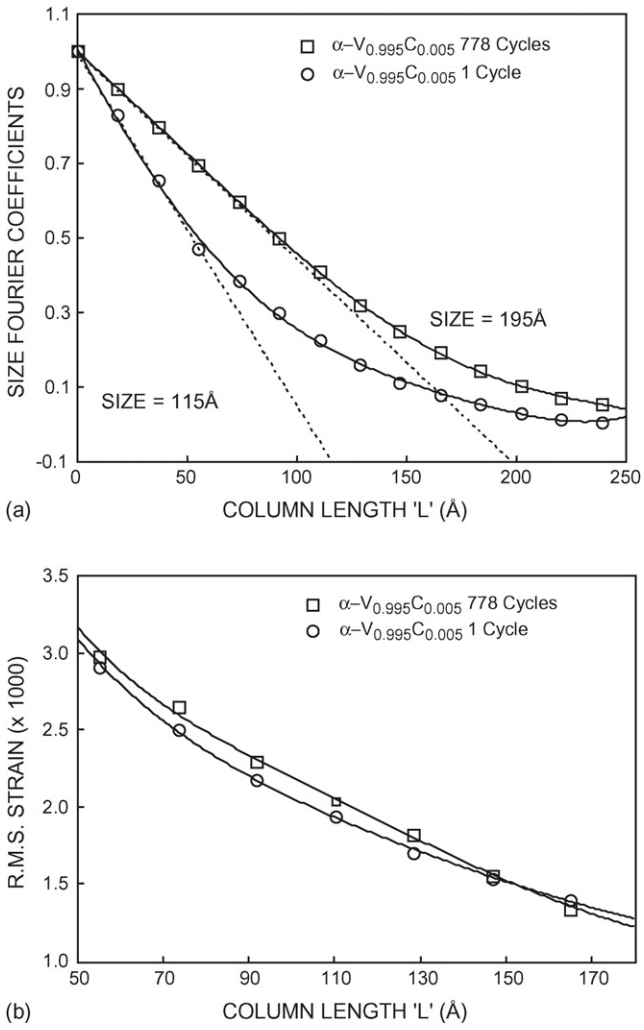

Fig. 10. (a) Effective domain size, D, along [1 1 0] and (b) microstrain in the terminal solid solution α-phase of V–0.5 at.%C after 1 and 778 cycles.

(to 1.9) after 1000 cycles. The two phase $\beta_2 + \gamma$ region also shows a slightly sloping plateau which showed an increase in the sloping factor ($\mathrm{d} \ln p/\mathrm{d}[\mathrm{H/M}]$ with increasing number of cycles. Similar sloping behavior has been reported for many hydrides such as $Zr(Fe_xCr_{1-x})_2$ [55]. The increases in the plateau slope associated with the decrease in hydrogen capacity after extended thermal cycling has also been observed in $LaNi_5$ and related intermetallics [34,55] but the hysteresis developed in these intermetallics is insignificant as compared to that observed with the V–0.5 at.%C alloy. An important thermodynamic quantity related to hysteresis is the free energy dissipation due to changes in the absorption and desorption pressures. It has been shown by Flanagan et al. [28] that this free energy loss due to pressure and solvus hysteresis is mathematically related as given below:

$$\Delta G_{\mathrm{loss}} = RT \ \ln\left(\frac{p_{\mathrm{f}}}{p_{\mathrm{d}}}\right) = RT \ \ln\left(\frac{a'}{a''}\right) \tag{8}$$

The free energy loss due to the pressure hysteresis developed due to thermal cycling, ΔG_{loss} ($\mathrm{J\,(mol\,H)^{-1}}$) as a function of number of cycles is given in Fig. 11(b). The ΔG_{loss} increases from $0.4\,\mathrm{J\,(mol\,H)^{-1}}$ for 20 cycles to $\sim 1.35\,\mathrm{J\,(mol\,H)^{-1}}$ for

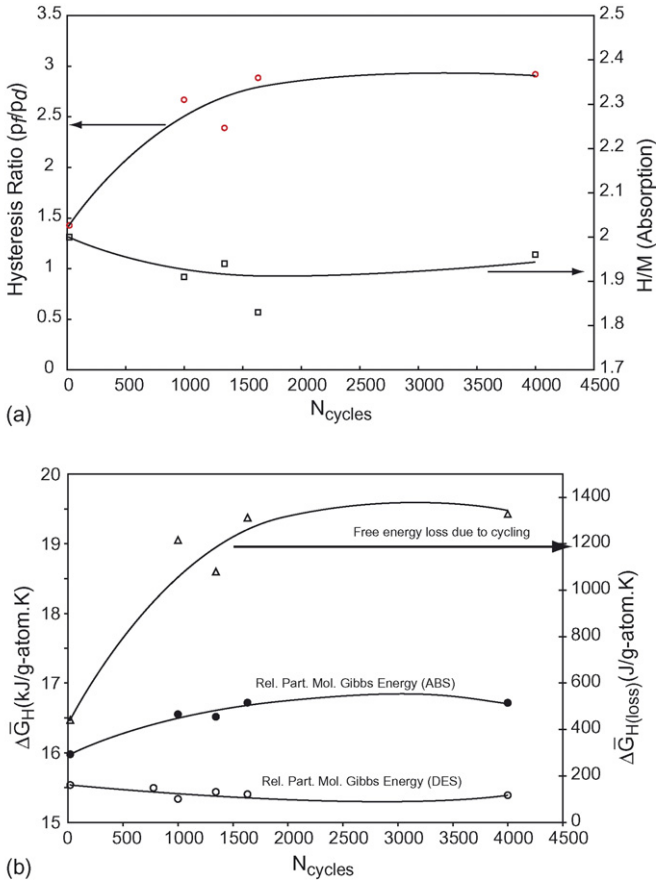

Fig. 11. (a) Hysteresis ratio and maximum absorption hydrogen capacity (H/M) as a function of the number of thermal cycles in V–0.5 at.%C hydride. (b) Free Energy loss due to thermal cycling as a function of number of cycles.

4000 cycles suggesting that there is an increased resistance to the hydrogen absorption in the cycled hydride. However, it is noted that this loss is associated only with the increase in absorption pressure as the dissociated pressure remains relatively unchanged for thermally cycled hydride (Fig. 9). This behavior is similar to that of VH_x [38]. The underlying causes of hysteresis are discussed later along with the hysteresis due to cold-work.

3.3. Effect of cold-working

3.3.1. Plateau pressures and microstrains

Cold-working V–0.5 at.%C alloy was found to have a large impact on the $\beta_2 - \gamma$ high-pressure isotherms. As shown in Fig. 12, the absorption plateau pressure at 298 K, increased from 396 to 600 kPa and more noticeably, the desorption plateau pressure also decreased from 280 to 153 kPa. This is in significant contrast to desorption behavior after thermal cycling. As discussed earlier, even after extensive thermal cycling, the desorption plateau pressures did not change appreciably. The hysteresis factor and the loss of hydrogen storage capacity also showed significant changes compared to thermal cycling and these are discussed in the following section.

Crystal structure analyses of the cold worked hydrides of V–0.5 at.%C sample, after hydrogen desorption to β_2-phase,

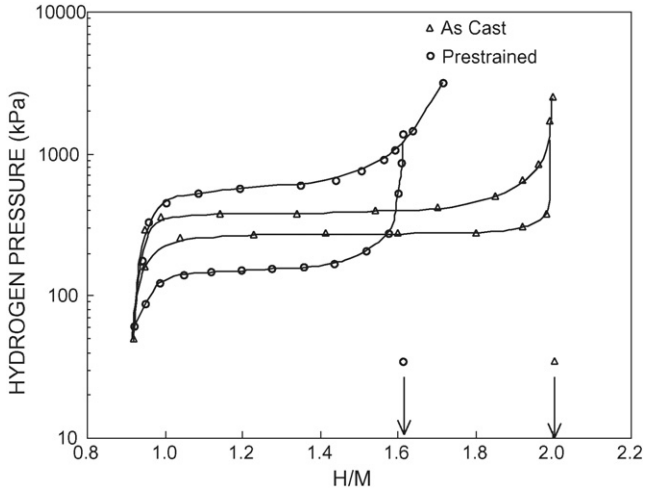

Fig. 12. Comparison of the isotherms obtained from the pre-strained and as-cast V–0.5 at.%C hydrides.

showed the presence of nearly 85% γ-phase. The domain size, *D*, along the [1 0 1] direction of the cold-worked β-phase is 215 ± 5.3 Å compared to 105 ± 2.8 Å for the as-cast β-phase hydride as shown in Fig. 13(a). This doubling of the domain size in the β-phase along [1 0 1] is a result of plastic deformation of the alloy prior to hydriding. The microstrain distributions in the β-phase hydrides are shown in Fig. 13(b). The associated microstrain along the [1 0 1] direction in the lattice of the as-cast β hydride was 3.5 (±0.10) × 10^{-3}, but the same β-phase hydride along [1 0 1] with prior cold-work had a microstrain of 2.2 (±0.08) × 10^{-3} at the respective half of the domain sizes. In the case of the γ-phase hydrides, the domain size was 438 Å as compared to the as-cast value of 452 Å along the [1 1 1] direction; showing little difference in domain size. The microstrain in the γ-phase of the as-cast alloy was 3.317 × 10^{-3}, which is greater than 2.369 × 10^{-3} for the cold-worked γ-phase. Dehydrogenation of the cold-worked binary γ − β-phases (not reported here) compared to the cold worked V–0.5 at.%C alloy before hydriding, showed an expected increase in the line width of the profile as compared to those of the as-cast samples. The domain size of the cold-worked α-phase V–0.5 at.%C alloy before hydriding was measured as 210 ± 5.7 Å which is comparable to the results of Aqua and Wagner [60] who reported an effective *D* value of 200 Å for pure vanadium α-phase. The associated microstrain distribution was 40% less than that of the pure vanadium and in the case of pure α-phase was 3.3 × 10^{-3} [60] while the value for the α-phase V–0.5 at.%C was 2.0 (±0.11) × 10^{-3} along [1 1 0].

3.3.2. Hysteresis in cold-worked hydrides

The hysteresis of the cold-worked/pre-strained samples increased significantly, and the H/M ratios decreased significantly, as compared to the non-strained sample as shown in Fig. 12. In this case, the alloy was subjected to only initial activation cycles and not cycled. The effective hydrogen absorption capacity reduced to about 1.6 for cold worked $V_{0.995}C_{0.005}$ alloy from 2 and the hysteresis ratio increased from 1.4 (as cast) to about 3.9. This significant increase is due to the cumulative effect of increase in absorption plateau pressure to 600 kPa and

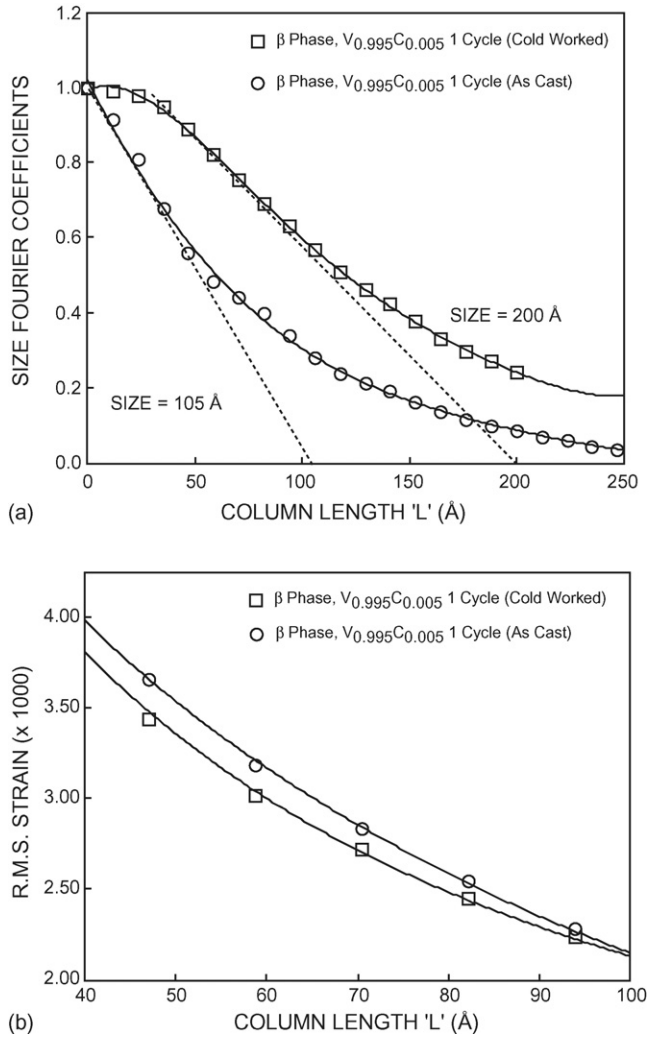

Fig. 13. (a) Effective domain size, *D*, along [1 0 1] and (b) microstrain in the cold-worked β-V–0.5 at.%C hydride after 1 cycle.

decrease in desorption plateau pressure to 153 kPa. Flanagan et al. [25] have observed similar effects in cold worked pure vanadium. The plastic deformation processes were apparently responsible for the increased hysteresis [25]. It is also suggested that dislocation motion during hydriding may contribute this considering that there is large volume change during cycling between $\beta_2 - \gamma$. It is quite likely that increased hysteresis was related to the plastic deformation introduced in the lattice by either cold work or thermal cycles. Therefore, a similarity in the microstrain distribution between the cold-worked and thermally cycled hydrides was observed that applies to both the β- and γ-phases. Birnbaum et al. [27], Flanagan et al. [28,29] and other researchers [61–67] proposed that metals and alloys undergo plastic deformations and dislocation creation both during hydride formation and decomposition. During the hydrogen absorption cycle, the β-phase is in a state of increasing compressive strain due to incipient formation of the γ-phase [65]. During hydrogen removal, both the β- and γ-phase matrices are increasingly relieved of compressive strain; i.e. desorption pressure remains the same. Thus, the higher pressure absorption isotherm is in a metastable condition and the absorption and desorption processes appear to incorporate a strain term. Thus, there was an increase in the domain size and decrease in microstrain due to prior cold work in the γ-phase hydrides. More recently, Schwarz and Khachaturyan [30] proposed a theory suggesting that hysteresis is an intrinsic thermodynamic phenomenon due to the coherent strains developed during hydride formation and decomposition. However, the applicability of this new theory to the pressure hysteresis developed due to thermal cycling in $V_{0.995}C_{0.005}H_x$ has not been explored at this time.

4. Conclusions

The present investigation represents an attempt to correlate the various macroscopic phenomenon of changes in hydriding characteristics (absorption/desorption pressures, hysteresis factor, sloping factor and reversible H/M capacity due to alloying, thermal cycling and cold-work) to the microscopic effects of changes in microstrains $\langle \varepsilon^2 \rangle^{1/2}$, effective domain sizes, and lattice parameters in V–0.5 at.%C alloy. The addition of 0.5 at.%C to pure vanadium increased the desorption plateau pressure by 40% for the $\gamma \rightarrow \beta$ transformations, indicating that carbon addition decreased the stability of the γ-phase, but apparently increased stability in the low pressure phase as indicated by a decrease in the plateau enthalpy. The plateau enthalpy and entropy values of the low pressure $\alpha - \beta_1$ region of $V_{0.995}C_{0.005}$ alloy showed a marked decrease compared to pure vanadium however the effect of carbon addition is minimal in the high pressure $\beta_2 - \gamma$ region. The relative partial molar enthalpy ($\Delta \bar{H}_H$) and entropy ($\Delta \bar{S}_H$) values as a function of hydrogen content in the condensed phase (N_H) in the $V_{0.995}C_{0.005}$–H system show a trend similar to that of pure vanadium.

Thermal cycling results clearly showed an increase in hysteresis due to increasing absorption pressures but virtually no change in the desorption pressures of the isotherms. The calculated free energy losses also increased with number of cycles suggesting an increasing resistance to hydrogen desorption. In general, the activation energy for the $\beta \rightarrow \gamma$ transformation was higher and became more pronounced after thermal cycling, yet the microstrains in the hydride phases decreased after thermal cycling (which was attributed to dynamic recovery processes during plastic deformation). Since the microstrain decreased and domain size increased in the β-hydride phases of both thermally cycled and pre-strained alloy, it is proposed that thermal cycling and cold-working have analogous behavior with respect to hydriding characteristics, *c*/*a* ratios, microstrain, and domain size effects in the β-phase. However, the values of desorption pressures and size-strain effects in the γ-phases were anomalous. The microstrains in the lattice of the dehydrogenated α-phases of V–0.5 at.%C alloys were similar to those of the intermetallics.

Acknowledgements

The authors wish to acknowledge the NASA Lyndon B. Johnson Space Center for supporting this research under NASA contract No. NAS 9-17549. We also thank Los Alamos National Laboratory for their support of this project. Many thanks to Keith Stever and Kay Blakely for help with X-ray instrumentation.

References

[1] R.C. Bowman Jr., B. Fultz, MRS Bull. 27 (9) (2002) 688–693.
[2] A.J. Maeland, in: M. Peruzzini, R. Poli (Eds.), Recent Adv. Hydride Chem., Elsevier, NY, 2001, p. 531 (and references therein).
[3] J.P. Blackledge, in: W.M. Mueller, J.P. Blackledge, G.G. Libowitz (Eds.), Metal Hydrides, Academic Press, NY, 1968, p. 1.
[4] R. Wiswall, in: G. Alefeld, J. Volkl (Eds.), Hydrogen in Metals. II. Application Oriented Properties, Springer-Verlag, Berlin, 1978, p. 208.
[5] R.L. Cohen, J.H. Wernick, Science 214 (1981) 1081.
[6] G. Sandrock, S. Suda, L. Schlapbach, in: L. Schlapbach (Ed.), Hydrogen in Intermetallic Compounds. II. Surface and Dynamic Properties: Applications, Springer-Verlag, Berlin, 1992, p. 197.
[7] F.E. Lynch, J. Less-Common Met. 172–174 (1991) 943.
[8] R.C. Bowman Jr., B.D. Freeman, E.L. Ryba, R.E. Spjut, E.A. Liu, J.M. Penso, F.E. Lynch, Z. Phys. Chem. 183 (1–2) (1994) 245.
[9] R.C. Bowman Jr., E.L. Ryba, B.D. Freeman, Adv. Cryogenic Eng. 39 (1994) 1499.
[10] J.S. Cantrell, R.C. Bowman Jr., A. Attalla, R.W. Baker, Z. Phys. Chem. 181 (1–2) (1993) 83.
[11] R.C. Bowman Jr., B.D. Freeman, J.R. Phillips, Cryogenics 32 (2) (1992) 127.
[12] S.N. Paglieri, D.R. Pesiri, R.C. Dye, S.A. Birdsell, R.C. Snow, in: Proceedings of the 19th Annual Conference on Fossil Energy Mater, May 9-11, 2005 Knoxville TN. http://www.ornl.gov/sci/fossil/pdf/Proceedings19/PAPERS/Session II/paglieri.pdf (accessed on July 26, 2006).
[13] D. Chandra, M. Coleman, J. Lamb, A. Sharma, W.N. Cathey, J.R. Wermer, S.N. Paglieri, R.C. Bowman Jr., F.E. Lynch, in: Proceedings of an International Conference on Solid State Hydrogen Storage-Materials And Applications, Hyderabad, January 2005, Int. J. Hydrogen Energy, in press.
[14] C.-H. Fagerstroem, F.D. Manchester, J.M. Pitre, in: F.D. Manchester (Ed.), Phase Diagrams of Binary Hydrogen Alloys, ASM International Materials Park, Ohio, 2000, pp. 273–292.
[15] P. Kofstad, W.E. Wallace, J. Am. Chem. Soc. 81 (1959) 5019.
[16] E. Veleckis, R.K. Edwards, J. Phys. Chem. 73 (1969) 683.
[17] R. Griffiths, J.A. Pryde, A. Righini-Brand, J. Chem. Soc. (London), Faraday Soc. Trans. I 68 (1972) 2344.
[18] K. Fujita, Y.C. Huang, M. Tada, J. Jpn. Inst. Met. 43 (1979) 601.
[19] J.J. Reilly, R.H. Wiswall Jr., Inorg. Chem. 9 (1970) 1678.
[20] W. Rummel, Siemens Forsch. Entwick. Ber. 10 (1981) 371.
[21] P. Meuffels, Bericht der KFA, Julich, No. 2081, 1986.
[22] T. Schober, Solid State Phenom. B49–B50 (1996) 357.
[23] A.Y. Esayed, D.O. Northwood, Int. J. Hydrogen Energy 17 (1992) 41.
[24] J.F. Lynch, G.G. Libowitz, A.J. Maeland, J. Less-Common Met. 103 (1984) 117.
[25] T.B. Flanagan, H. Noh, J.D. Clewley, R.C. Bowman Jr., Scr. Metal. Mater. 28 (1993) 355.
[26] N.A. Scholtus, W.K. Hall, J. Chem. Phys. 39 (1963) 868.
[27] H.K. Birnbaum, M.L. Grossbeck, M. Amano, J. Less-Common Met. 49 (1976) 357.
[28] T.B. Flanagan, W.A. Oates, S. Kishimoto, Scr. Metall. 16 (1982) 293.
[29] T.B. Flanagan, B.S. Bowerman, G.E. Biehl, Scr. Metall. 14 (1980) 443.
[30] R.B. Schwarz, A.G. Khachaturyan, Acta Mater. 54 (2006) 313.
[31] T.B. Flanagan, J.D. Clewley, T. Kuji, C.N. Park, D.H. Everett, J. Chem. Soc., Faraday Trans. I 82 (1986) 2589.
[32] T.B. Flanagan, C.-N. Park, W.A. Oates, Prog. Solid State Chem. 23 (1995) 291.
[33] T.B. Flanagan, W.A. Oates, J. Alloys Compd. 404–406 (2005) 16.
[34] S. Lambert, D. Chandra, W.A. Cathey, F.E. Lynch, R.C. Bowman Jr., J. Alloys Compd. 187 (1992) 133.
[35] D. Chandra, W.N. Cathey, D. Clare, H. Mandalia, W. Chien, J.R. Wermer, J.S. Holder, W.C. Mosley, in: R. Bautista, B. Mishra (Eds.) Rare Earths IV, TMS Conference Proceedings, 2000, pp. 78–97.
[36] S. Bagchi, D. Chandra, W. Cathey, R. Schwartz, R.C. Bowman Jr., F.E. Lynch, in: R. Bautista, C. Bound, T. Ellis, B. Kilbourn (Eds.), Rare Earths III, TMS Conference Proceedings, 1997, pp. 75–85.
[37] D. Chandra, S. Bagchi, S.W. Lambert, W.N. Cathey, F.E. Lynch, R.C. Bowman Jr., J. Alloys Compd. 199 (1–2) (1993) 93.
[38] R.C. Bowman Jr., F.E. Lynch, R.W. Marmaro, C.H. Luo, B. Fulz, J.S. Cantrell, D. Chandra, Z. Phys. Chem. 181 (1–2) (1993) 269.
[39] R.W. Marmaro, F.E. Lynch, D. Chandra, Investigation of Long Term Stability in Metal Hydrides, NAS9-18175 by HCI, 12410 North Dumont Way, Littletown, CO 80125, November, 1991.
[40] S. Kumar, R. Balasubramaniam, Int. J. Hydrogen Energy 20 (1995) 211.
[41] A. Sharma, Effect of thermal cycling and cold-work on V0.995 C0.005 hydrides, Thesis (MS) 2908, University of Nevada, Reno, 1992.
[42] J.S. Cantrell, R.C. Bowman Jr., J. Alloys Compd. 293–295 (1999) 156.
[43] A.J. Maeland, G.G. Libowitz, J.F. Lynch, G. Rak, J. Less-Common Met. 104 (1984) 133.
[44] G.G. Libowitz, A.J. Maeland, Mater. Sci. Forum 31 (1988) 177.
[45] A. Kagawa, E. Ono, T. Kusakabe, Y. Sakamoto, J. Less-Common Met. 172–174 (1991) 64.
[46] H. Yukawa, M. Takagi, A. Teshima, M. Morinaga, J. Less-Common Met. 330–332 (2002) 105.
[47] H. Yukawa, M. Takagi, A. Teshima, M. Morinaga, J. Less-Common Met. 337 (2002) 264.
[48] W. Rostoker, The Metallurgy of Vanadium, Wiley, NY, 1958.
[49] E.I. Sokolova, L.N. Padurets, A.L. Shilov, N.T. Kuznetsov, M.E. Kost, Russ. J. Inorg. Chem. 33 (1988) 275.
[50] M.E. Kost, L.N. Padurets, E.I. Sokolova, A.L. Shilov, Dokl. Akad. Nauk. S.S.S.R. 254 (1980) 1134.
[51] J. Cohen, Line Profile Analyses Workshop Notes, Northwestern University, 1984.
[52] B.E. Warren, X-Ray Diffraction, Addison-Wesley, Reading, MA, 1969.
[53] Th.H. De Keijser, J.J. Langford, E.J. Mittemeijer, A.B.P. Vogel, J. Appl. Cryst. 15 (1982) 308.
[54] W. Luo, J.D. Clewley, T.B. Flanagan, J. Chem. Phys. 93 (9) (1990) 6710.
[55] S. Qian, D.O. Northwood, J. Less-Common Met. 147 (1989) 149.
[56] P.D. Goodell, J. Less-Common Met. 99 (1984) 1.
[57] H. Uchida, H. Uchida, Y.C. Huang, J. Less-Common Met. 101 (1984) 459.
[58] K. Nomura, H. Uruno, S. Ono, H. Shinozuka, S. Suda, J. Less-Common Met. 107 (1985) 221.
[59] Y. Josephy, E. Bershadshky, M. Ron, J. Less-Common Met. 172–174 (1991) 997.
[60] E.N. Aqua, C.N.J. Wagner, Phil. Mag. 9 (1964) 565.
[61] C.N. Park, T.B. Flanagan, Scr. Metall. 18 (1984) 683.
[62] T.B. Flanagan, W.A. Oates, J. Less-Common Met. 100 (1984) 299.
[63] B.S. Bowerman, C.A. Wulff, G.E. Biehl, T.B. Flanagan, J. Less Common Met. 73 (1980) 1.
[64] T. Kuji, T.B. Flanagan, Y. Sakamoto, M. Hasaka, Scr. Metall. 19 (1985) 1369.
[65] C.E. Lundin, F.E. Lynch, in: A.F. Andresen, A.J. Maeland (Eds.), Hydrides for Energy Storage, Pergamon, Oxford, 1978, p. 395.
[66] S. Qian, D.O. Northwood, Int. J. Hydrogen Energy 13 (1988) 25.
[67] D. Wang, T.B. Flanagan, T. Kuji, Phys. Chem. Chem. Phys. 4 (2002) 4244.